Supplemental Material: Control of nonlocal magnon spin transport via magnon drift currents

Richard Schlitz,[1,2,*] Saül Vélez,[1,†] Akashdeep Kamra,[3,4] Charles-Henri Lambert,[1]
Michaela Lammel,[5,6] Sebastian T. B. Goennenwein,[2,6] and Pietro Gambardella[1]

[1]*Department of Materials, ETH Zürich, 8093 Zürich, Switzerland*
[2]*Institut für Festkörper- und Materialphysik, Technische Universität Dresden and Würzburg-Dresden Cluster of Excellence ct.qmat, 01062 Dresden, Germany*
[3]*Center for Quantum Spintronics, Department of Physics, Norwegian University of Science and Technology, 7491 Trondheim, Norway*
[4]*Condensed Matter Physics Center (IFIMAC) and Departamento de Física Teórica de la Materia Condensada, Universidad Autónoma de Madrid, E-28049 Madrid, Spain*
[5]*Leibniz Institute for Solid State and Materials Research Dresden (IFW Dresden), Institute for Metallic Materials, 01069 Dresden, Germany*
[6]*Department of Physics, University of Konstanz, 78457 Konstanz, Germany*

(Dated: May 11, 2021)

S1. TRANSMISSION ELECTRON MICROSCOPY OF THE GGG/YIG INTERFACE

To exclude the formation of a $Gd_3Fe_5O_{12}$ interface layer at the YIG/GGG interface we have performed a spatially resolved energy dispersive X-ray spectroscopy (EDS) analysis using a dual 100 mm window-less silicon drift detector in a JEOL JEM F200 microscope. To mitigate the impact of Ga implantation during the sample preparation via focused ion beam thinning, low kV Ar-ion milling was used to thin the lamella to final thickness.

Figure S1 summarizes the results of the cross-section EDS analysis performed on a sample grown by liquid phase epitaxy. The EDS line profiles show that all elements transition at the same interface, thus excluding the formation of a $Gd_3Fe_5O_{12}$ layer. In contrast, in Ref. [1] a shift of the crossing point of Gd by ~ 2.5 nm towards the YIG layer was observed.

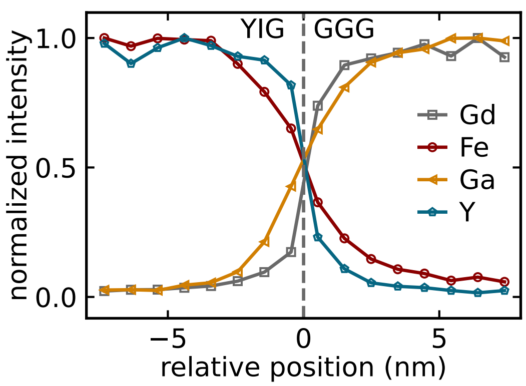

FIG. S1: Line profiles of the elemental EDS maps taken on a sample grown by liquid phase epitaxy. No shift of the Gd signal towards the YIG layer (left) is found, so that we exclude the formation of a $Gd_3Fe_5O_{12}$ layer at the interface. Note that the residual Fe signal in the GGG layer is due to X-rays from the Fe-rich pole pieces that are generated by scattered electrons.

* richard.schlitz@mat.ethz.ch

† saul.velez@mat.ethz.ch, Present address: Condensed Matter Physics Center (IFIMAC) and Departamento de Física de la Materia Condensada, Universidad Autónoma de Madrid, E-28049 Madrid, Spain

S2. CURRENT DEPENDENCE OF $A_{1\omega}$ AND $S_{1\omega}$

To evaluate the current dependence of the diffusive and the drift contribution to the nonlocal magnon transport, we performed angular scans for different currents I. The resulting drift $\Delta R_{1\omega}$ and diffusive $\Sigma R_{1\omega}$ contributions are shown in Fig. S2a and b, respectively. To obtain the amplitudes, the data are fitted with the function $A_{1\omega}\sin^2(\alpha)\cos(\alpha)$ (for $\Delta R_{1\omega}$) or $S_{1\omega}\sin^2(\alpha)$ (for $\Sigma R_{1\omega}$). When plotted, the amplitudes $A_{1\omega}$ and $S_{1\omega}$ of the drift and diffusive contribution reveal a parabolic dependence on the current (cf. Fig. S2c). Higher currents generate more heat via ohmic losses, leading to an increase of the (time averaged) temperature by an amount $\Delta T \propto I^2$. The diffusive contribution to the nonlocal signal was shown to increase with a power-law T^α, where $\alpha \sim 1$ at room temperature [2]. Consequently, the amplitude $S_{1\omega}$ is expected to increase linearly with ΔT and thus depends on the square of the current. The same is observed for $A_{1\omega} \propto S_{1\omega}$, which also depends on the magnitude of the diffusive contribution [see Eq. (7) in the main text]. In contrast, the ratio $|A_{1\omega}/S_{1\omega}|$ which is proportional to $d_{\mathrm{nl}} v_{\mathrm{DMI}} \tau_{\mathrm{m}}/2\lambda_0^2$ is independent of the current to within our experimental errors. We also point out that, as the signal increases towards higher temperatures, measurements at elevated temperatures might be beneficial to reveal the effect with higher sensitivity.

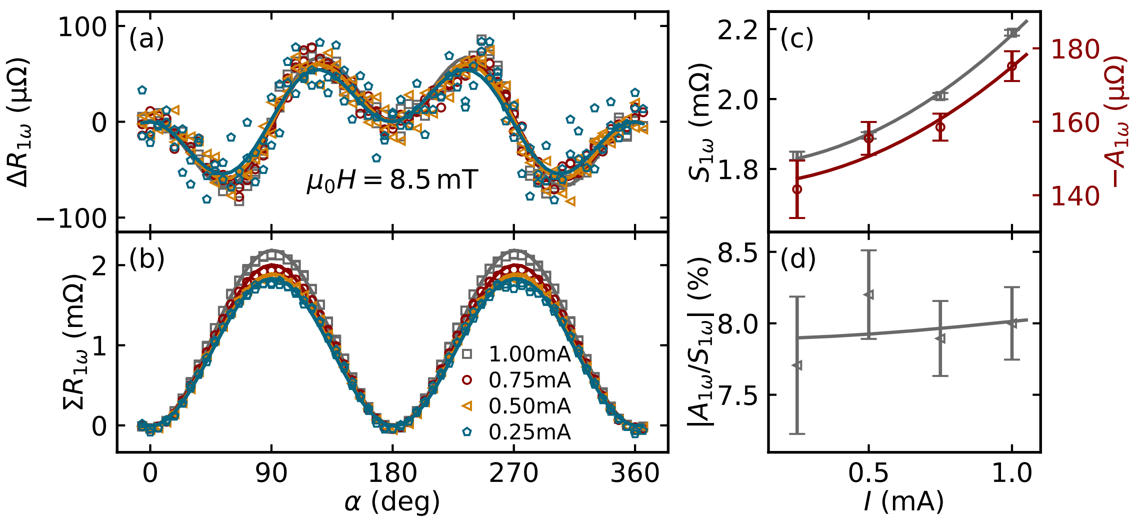

FIG. S2: (a) $\Delta R_{1\omega}$ as a function of the angle measured for several different currents. The solid lines correspond to fits of the $\sin^2(\alpha)\cos(\alpha)$ angle dependence. (b) Corresponding data for $\Sigma R_{1\omega}$, where the solid lines are $\sin^2(\alpha)$ fits. (c) The amplitudes $S_{1\omega}$ (gray symbols) and $A_{1\omega}$ (red symbols) of $\Sigma R_{1\omega}$ and $\Delta R_{1\omega}$, respectively plotted as a function of the current. The gray and red line are parabolic fits. (d) $|A_{1\omega}/S_{1\omega}|$ is independent of the current within the error. The solid line is the ratio of the two parabolic fits in panel c.

S3. SECOND HARMONIC NONLOCAL SIGNAL

To determine whether there is a contribution of the DMI also to the second harmonic nonlocal signal, we show $R_{2\omega,\mathrm{L}}$ and $R_{2\omega,\mathrm{R}}$ obtained on the left and right wire, respectively, in Fig. S3a. Note that we define the second harmonic signal as $R_{2\omega} = V_{2\omega}/I_0$, in analogy to the first harmonic signal $R_{1\omega}$. Both curves show a dominant $\sin(\alpha)$ dependence on the external magnetic field direction. This dependence is expected for a signal that is due to long range magnon currents which are thermally excited below the injector [3]. On the other hand, the spin Seebeck effect caused by the local thermal gradients below the detector wires can give rise to an identical dependence. In addition, we observe a clear difference between the signal on the left and right wire. To disentangle the symmetric and antisymmetric effects, we again follow the procedure detailed in the main manuscript, i.e., we take the difference and the sum of $R_{2\omega,\mathrm{L}}$ and $R_{2\omega,\mathrm{R}}$, respectively. The resulting $\Delta R_{2\omega} = (R_{2\omega,\mathrm{L}} - R_{2\omega,\mathrm{R}})/2$ and $\Sigma R_{2\omega} = (R_{2\omega,\mathrm{L}} + R_{2\omega,\mathrm{R}})/2$ are shown in Fig. S3b and c, respectively. $\Delta R_{2\omega}$ exhibits a $\cos(\alpha)\sin(\alpha)$ angular dependence, whereas $\Sigma R_{2\omega}$ can be described by a $\sin(\alpha)$ dependence. As described above the latter is consistent with thermally driven magnon transport or the spin Seebeck effect. In contrast, the $\cos(\alpha)\sin(\alpha)$ dependence has the symmetry of the spin Nernst effect (SNE) appearing in the transport signal due to the modulation of the boundary conditions for the spin current at the YIG interface [4]. To motivate why the SNE appears in the antisymmetric signal $\Delta R_{2\omega}$, the direction of the in-plane thermal gradients needs to be considered: The in-plane thermal gradients at the position of the left and right electrode both point towards the central electrode and are thus opposite to each other. Consequently, also the SNE signal, which will invert when the thermal gradient is inverted, is opposite for the two electrodes. Since one would naively expect the DMI contribution to the thermal transport effect to have the same $\cos(\alpha)\sin(\alpha)$ angular dependence, a possible contribution of the DMI to the thermally driven magnon transport cannot be straightforwardly identified from the data.

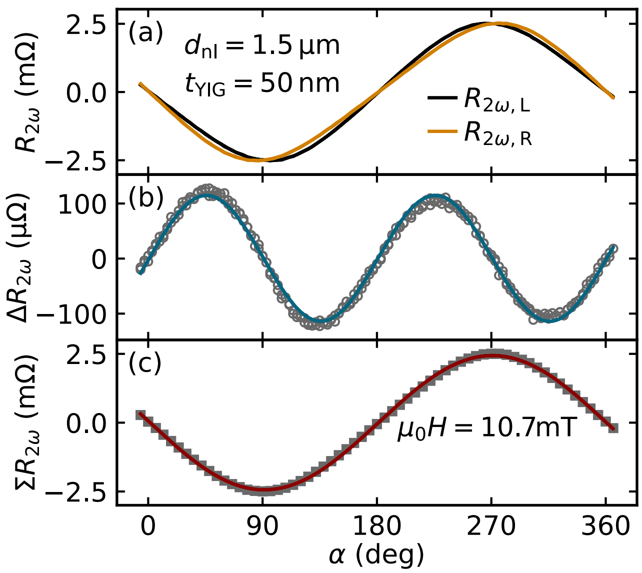

FIG. S3: (a) The second harmonic signal $R_{2\omega,\mathrm{L}}$ detected on the left wire (black line) and $R_{2\omega,\mathrm{R}}$ detected on the right wire (yellow line) are shown as a function of the angle α between the current direction and the magnetic field. (b) $\Delta R_{2\omega} = (R_{2\omega,\mathrm{L}} - R_{2\omega,\mathrm{R}})$ can be described by a $\cos(\alpha)\sin(\alpha)$ angle dependence (blue line). (c) $\Sigma R_{2\omega} = (R_{2\omega,\mathrm{L}} + R_{2\omega,\mathrm{L}})$ has a $\sin(\alpha)$ shape (red line) as expected for thermally driven magnon transport or the spin Seebeck effect.

S4. ORIENTATION OF THE MAGNETIC FIELD

To provide full traceability of the sign of the DMI constant in our definition [see Eq. (1) in the main text], we have verified the orientation of the magnetic field starting from a reference coil and summarized all vector directions in Fig. S4. A positive current is applied to the reference coil and the coil is inserted into the electromagnet used for the transport measurements. The orientation of the magnetic field in the reference coil is thus defined by the right-hand rule (cf. Fig. S4a). In the following, we have verified that the coil is not expelled from the magnet when a positive magnetic field is applied (i.e., parallel to the magnetic field generated by the reference coil). In contrast, when the external magnetic field is inverted, the reference coil is pushed out of the pole gap of the magnet.

The magnetization is aligned parallel to the magnetic field and the interfacial symmetry breaking is defined by the GGG/YIG interface normal $\hat{\mathbf{z}}$, which coincides with the surface normal of the film $\mathbf{n}$ (cf. Fig. S4b).

To completely pin down the sign of the DMI constant, it is important to note that we study transport from the central wire to the left wire so that the magnon wave vector $\mathbf{k}$ is parallel to $\mathbf{y}$ (cf. Fig. S4c).

[1] J. M. Gomez-Perez, S. Vélez, L. McKenzie-Sell, M. Amado, J. Herrero-Martín, J. López-López, S. Blanco-Canosa, L. E. Hueso, A. Chuvilin, J. W. A. Robinson, and F. Casanova, Physical Review Applied **10**, 044046 (2018).

[2] S. T. B. Goennenwein, R. Schlitz, M. Pernpeintner, K. Ganzhorn, M. Althammer, R. Gross, and H. Huebl, Applied Physics Letters **107**, 172405 (2015).

[3] L. J. Cornelissen, J. Liu, R. A. Duine, J. B. Youssef, and B. J. van Wees, Nature Physics **11**, 1022 EP (2015).

[4] S. Meyer, Y.-T. Chen, S. Wimmer, M. Althammer, T. Wimmer, R. Schlitz, S. Geprägs, H. Huebl, D. Ködderitzsch, H. Ebert, G. E. W. Bauer, R. Gross, and S. T. B. Goennenwein, Nature Materials **16**, 977 (2017).

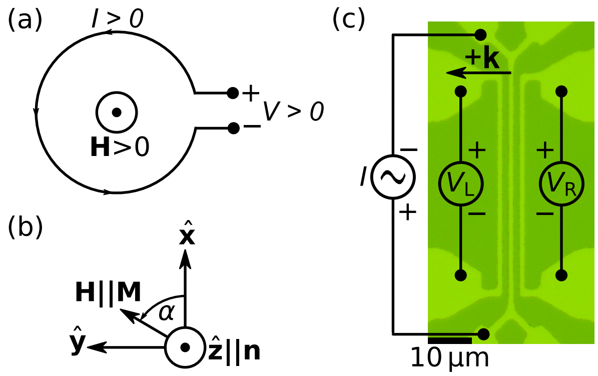

FIG. S4: (a) The orientation of a positive magnetic field is defined by the right hand rule. (b) The coordinate system, where we give the angle α between the current direction and the magnetic field (with parallel magnetization). We assume that the interface normal relevant for the DMI ($\hat{\mathbf{z}}$) points along the surface normal of the film $\mathbf{n}$. (c) The magnon wave vector $\mathbf{k}$ is shown with respect to the coordinate system in panel (b) and the contact polarities.